

Article

Green Synthesis of Gold and Copper Nanoparticles by *Lannea discolor*: Characterization and Antibacterial Activity

Unarine Rambau ¹, Nndivhaleni Anox Masevhe ^{1,*} and Amidou Samie ²

¹ Department of Biological Sciences, Faculty of Science, Engineering and Agriculture, University of Venda, Thohoyandou 0950, South Africa; unarambau@gmail.com

² Department of Biochemistry and Microbiology, Faculty of Science, Engineering and Agriculture, University of Venda, Thohoyandou 0950, South Africa

* Correspondence: nndivhaleni.masevhe@univen.ac.za

Abstract: Green synthesis using plant extracts has emerged as an eco-friendly, clean, and viable alternative to chemical and physical approaches. Herein, the leaf, stem, and root extracts of *Lannea discolor* were utilized as a reducing and stabilizing agent in synthesizing gold (AuNPs) and copper (CuNPs) nanoparticles. The formation of AuNPs and CuNPs, confirmed by their color change, was characterized by UV-Vis spectroscopy (UV-Vis), scanning electron microscopy analysis, and energy-dispersive X-ray (SEM-EDX), transmission electron microscopy (TEM), and Fourier-transform infrared spectroscopy (FTIR), coupled with minimum inhibitory concentration (MIC) antibacterial assays. Gold nanoflowers (AuNFs), NPs, and CuNPs peaked at wavelengths of 316, 544, and 564 nm, respectively. TEM showed unexpected nanoflowers (30–97 nm) in the leaf extracts and spherical NPs (10–33 nm; 9.3–37.5) from stem and root extracts, while spherical CuNPs (20–104 nm) were observed from all the extracts. EDX confirmed the presence of metal salts, and FTIR revealed stable capping agents. AuNPs and NFs from *L. discolor* extracts showed appreciable antibacterial activity against *Staphylococcus aureus* (ATCC 25923), *Escherichia coli* (ATCC 25922), *Pseudomonas aeruginosa* (ATCC 27853), *Klebsiella pneumoniae* (ATCC 700603), and *Bacillus subtilis* (ATCC 6633) when compared to the plant extracts. At the same time, none was observed from the CuNPs. These AuNPs and CuNPs are particularly appealing in various biomedical and conductivity manufacturing applications due to their shapes and sizes and economical and environmentally friendly production. To our knowledge, this is the first study of the synthesis of gold and copper nanoparticles from *L. discolor*.

Keywords: gold nanoflowers; plant extracts; nanosynthesis; transmission electron microscopy (TEM)



Citation: Rambau, U.; Masevhe, N.A.; Samie, A. Green Synthesis of Gold and Copper Nanoparticles by *Lannea discolor*: Characterization and Antibacterial Activity. *Inorganics* **2024**, *12*, 36. <https://doi.org/10.3390/inorganics12020036>

Academic Editor: Carlos Martínez-Boubeta

Received: 24 November 2023

Revised: 7 January 2024

Accepted: 9 January 2024

Published: 24 January 2024



Copyright: © 2024 by the authors. Licensee MDPI, Basel, Switzerland. This article is an open access article distributed under the terms and conditions of the Creative Commons Attribution (CC BY) license (<https://creativecommons.org/licenses/by/4.0/>).

1. Introduction

Nanotechnology, a globally active research discipline, is rapidly progressing, with nanoparticles being a topic of interest since the 1970s [1]. Nanoparticles (NPs) are microscopic particles with at least one dimension less than 100 nm. They can be categorized into different types according to morphology, size, physicochemical properties, and the type of precursor from which they are synthesized [2]. Metal nanoparticles (NPs) like gold and copper are created from metal precursors using synthetic or chemical methods, which may use environmentally unfriendly reducing agents [3]. This has resulted in scientists turning to safer synthesis methods by employing biological reductants such as bacterial, fungal, and plant material to curb any possible negative effects from nanosynthesis [4]. Gold nanoparticles (AuNPs) are used in various fields, such as gene therapy, protein delivery, cancer diagnosis, photodermal and photodynamic therapy, the delivery of antitumor agents, and DNA detection and catalysis [5]. Ancient Indian healers used them for asthma and arthritis. Later, the Romans used them for cathedral glassware decoration. Recently, they have functioned as photocatalytic air purifiers, gaining significant therapeutic applications [6]. AuNPs are compatible with living tissue, producing no toxic or immunological response.

They have been used as nanocarriers for anti-inflammatory drugs due to their small sizes, improved stability, and adsorption efficiencies [7,8]. Plant extracts have gained attention as reducing agents for AuNP synthesis due to their low toxicity, eco-friendliness, and simplicity of production [4,9]. Various plants, such as *Anacardium occidentale* [10], *Spondias dulcis* [11], and *Pistacia chinensis* [12], have been reported to be effective in reducing gold ions into differently shaped and sized nanoparticles. Nanotechnology has enabled the development of modern techniques for nanoscale copper generation over the past decade [13]. Copper nanoparticles (CuNPs) are gaining attention due to their ease of availability and economic feasibility, unlike some noble metals that are resistant to oxidation and easy to work with but may be costly to acquire, such as silver, gold, and platinum. They are widely utilized in cancer imaging due to their efficient light-to-heat transformation under near-infrared laser irradiation [13]. Other uses include enhancing heat transfer liquids, photonic devices, sensors, and electrochemical devices [14,15]. CuNPs, with their unique properties, have gained significant applications in various industries such as cosmetology, agriculture, food, textiles, and construction [16,17]. In several studies, CuNPs providing higher environmental mobility were synthesized using various plant extracts, including *Cissus vitiginea* [17], *Zingiber officinalis* and *Curcuma longa* [18], *Brassica oleracea* [19], and *Hyptis suaveolens* (L.) [20].

Lannea discolor from the family Anacardiaceae is a deciduous tree that usually grows up to 15 m on rocky slopes or sandy soil. The leaves are discoloured, having a green-colored adaxial surface and a gray, dense trichome layer on the abaxial surface. Its traditional uses include treatment for diarrhea, stomach complaints, and an array of infections [21]. The plant's pharmacological activities are purported to result from various secondary metabolites such as phenolic flavonoids, alkaloids, and tannins [22]. CuNPs are a stable substitute for gold, so they may be a low-cost replacement for unattainable precious metals. Conclusively, in this study, all NPs were characterized by UV-Vis spectrometry, FTIR spectroscopy, SEM-EDX, and TEM to investigate the optical, morphology, and elemental composition and the antibacterial activities of nanoparticles, respectively.

2. Results and Discussion

2.1. Visual and UV-Vis Spectroscopic Analysis

This study is a simple and sustainable method for synthesizing AuNPs and CuNPs by mixing AuCl_4 and CuSO_4 solutions with the methanol, acetone, and water extracts of *Lannea discolor*. Following the incubation of AuCl_4 and CuSO_4 solutions with extracts, solutions went from dark yellow to grayish for the leaves (Figure 1A,C), and intense violet for the stem and root was observed (Figure 1B,D). When exposed to CuSO_4 , the extracts changed from their usual color to a more intensified burnt orange for the leaves (Figure 1E,G) and a brown to a darker brown for the stem and root (Figure 1H). This was observed in all extracts from all solvents.

UV-Vis representative absorption spectra for the AuNPs and CuNPs are shown in Figure 2A,B. The absorption peak for the AuNPs from stem and root extracts had a maximal absorption at 544 nm, while the leaf extracts' NF solutions peaked at 316 nm. Consistent peaks were observed for the AuNPs and NFs acquired from methanol, acetone, and water extracts. Similar results were observed in other studies [23,24]. As much as the UV-Vis characteristic wavelength of AuNPs has been used to validate the synthesis of NPs, certain peaks may also be attributed to the size and shape of the nanoparticles. The NP solution's color change to gray is due to Ostwald ripening, a well-understood phenomenon involving the redeposition of smaller nanoparticles to larger ones to form popcorn, flower, or starlike shapes [25]. Correspondingly, the pointed peaks (at both 25 °C and 80 °C) observed in the NPs obtained from the leaf extracts (Figure 2A) confirm a different morphology in contrast to the NPs obtained from the stem and root extracts. This can be observed in the UV-Vis peaks of the rest of the samples in this study (Figure S1). Studies show that spherical AuNPs appear red but turn blue or gray when they form NFs [26,27].

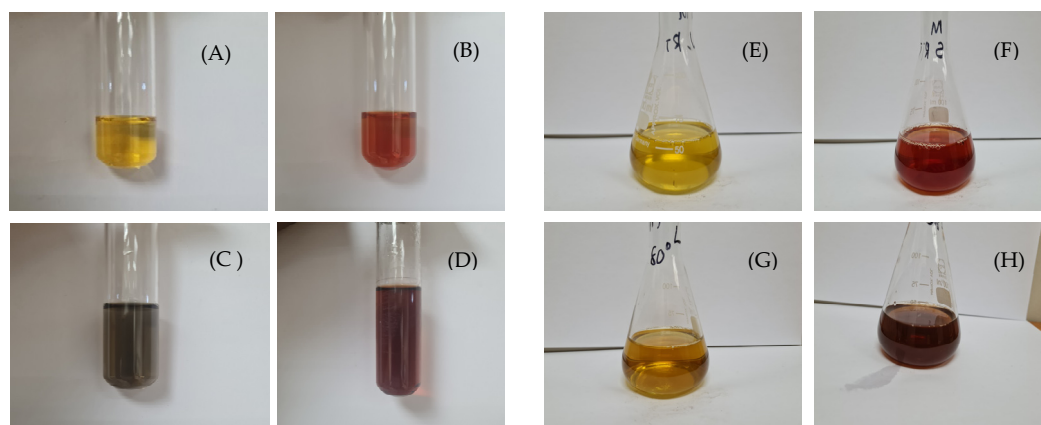


Figure 1. Visual representation of *Lannea discolor* extracts before NP synthesis. (A) Leaf, (B) stem and root, (C) AuNPs from leaves, and (D) AuNPs from stem and root bark. (E,F) are solutions before CuNP synthesis. CuNPs from leaf (G) and stem and root (H) after synthesis.

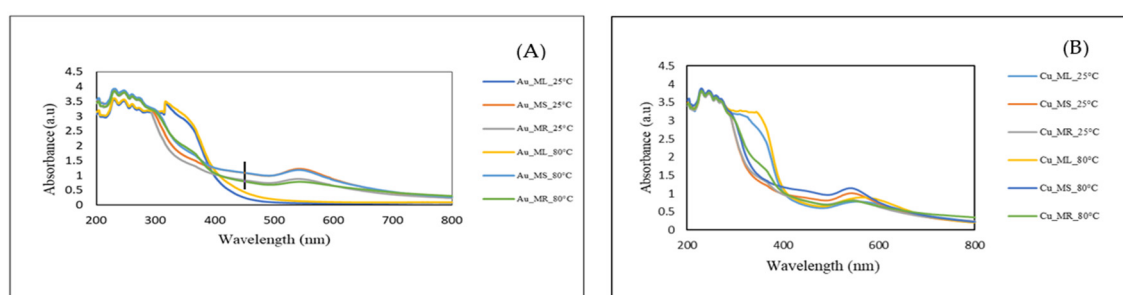


Figure 2. Representative UV-Vis spectra of SPR bands representing *Lannea discolor* (A) AuNPs/NFs and (B) CuNPs from methanol extracts. Sample keys: ML = Methanol leaf; MS = Methanol stem; MR = methanol root.

The CuNPs display an absorption peak at 556–564 nm for leaves and 540–546 nm for stems and roots. As Figure 2B shows, the increase in the temperature did not significantly reduce or increase the adsorption and synthesis of CuNPs. It is reported in the literature that the surface plasmon resonance band of CuNPs provides absorption from 500 to 600 nm [28]. Therefore, the UV-Vis peak acquired in this region after synthesis confirms the formation of CuNPs.

2.2. The Morphology of the Synthesized Nanoparticles Using Scanning Electron Microscopy and Energy-Dispersive X-ray Analysis

The SEM analysis in Figure 3A shows aggregated AuNPs that were present from all leaf extracts, thus confirming the influence of the leaf extracts from all extracts on the morphology observed. The fluorescence emission of the AuNPs synthesized using stem methanol extract is observed in Figure 3B inset. Under light irradiation, AuNPs emit fluorescence, a characteristic suggested to confer phototherapy potential and show the possible optical properties of the AuNPs [29].

The CuNPs from the leaf, stem, and root extracts were spherical (Figures 4A and S3) and aggregated, resulting from static tension [30]. Furthermore, unexpected sintering is observed in Figure 4B after exposure to heat. Sintering involves joining nanoparticles into a solid mass due to temperatures less than 250 °C, pressure, and leftover alcohols during evaporation [31]. As such, during both synthesis and drying, the CuNPs undergo sintering, and the well-connected features are observed in Figure 4B. Sintering techniques have been standardized to produce chemically synthesized CuNPs for copper inks used in conductivity [31,32]. Yet, no work has been reported employing a sintering temperature as low as 60 °C for CuNPs from *Lannea discolor* extracts. The literature reports that the optical

and electronic properties of NPs depend on morphology [32,33], granting CuNPs potential in these applications.

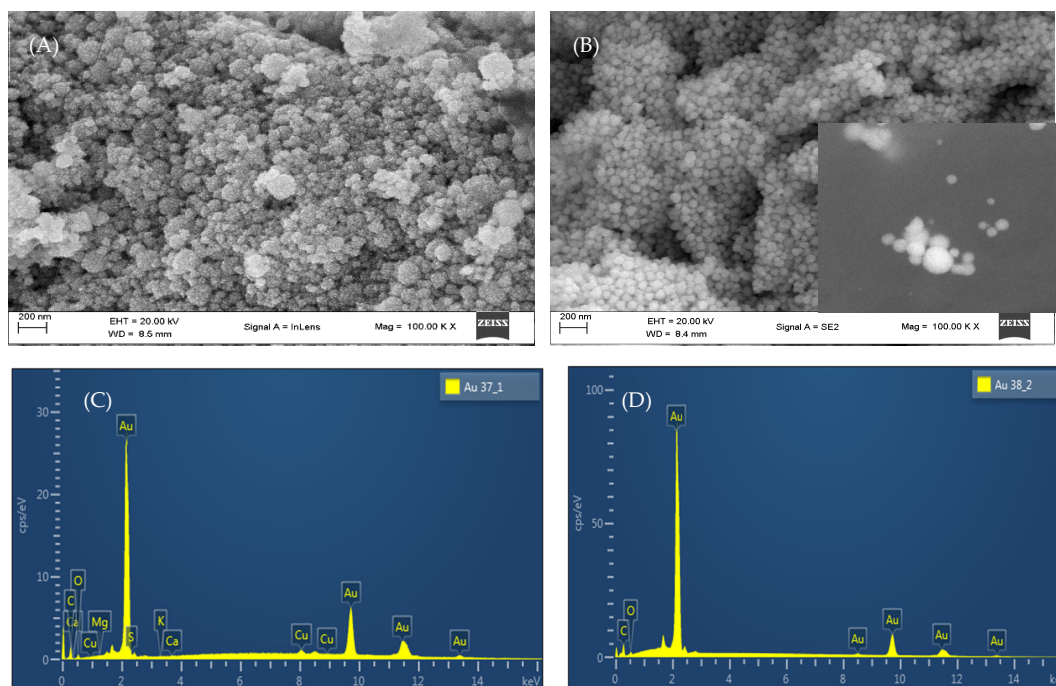


Figure 3. Representative SEM images of AuNFs from methanol leaf extracts. (A,B) AuNPs from methanol stem extract of *L. discolor* and (C,D) EDX spectra. Inset of (B) is image of fluorescence emission from AuNPs. Insets of (C,D) contain graphs of the abundance of Au to validate the formation of AuNFs and NPs.

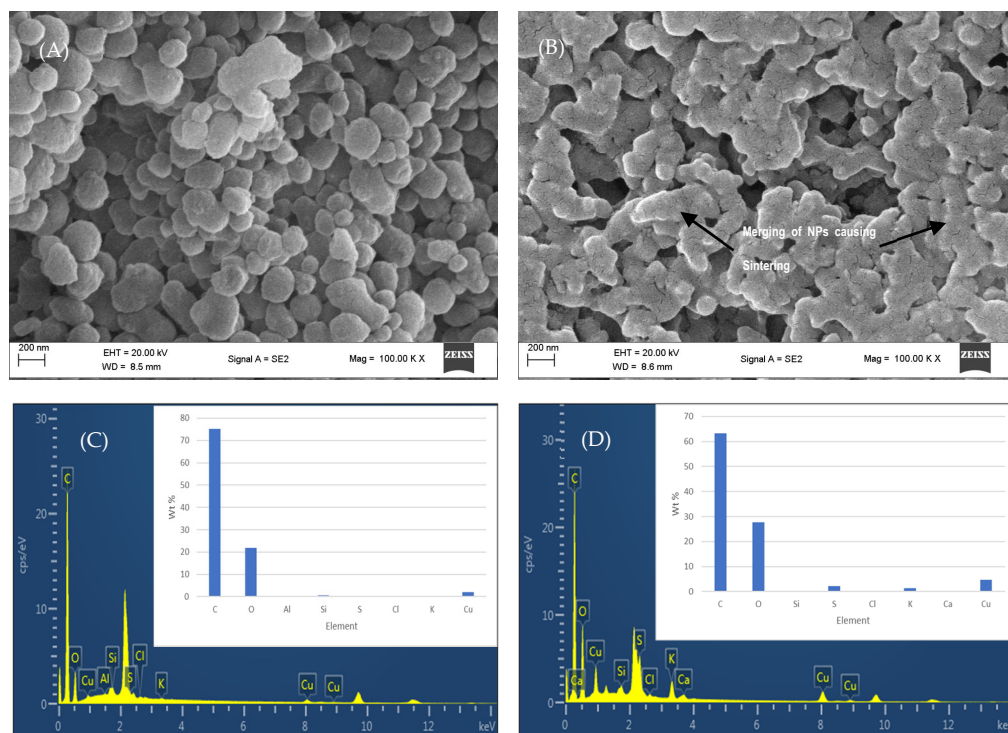


Figure 4. Representative SEM images and EDX spectra of CuNPs from the leaf methanol extracts of *Lanena discolor*. (A) Nanoparticles synthesized at 25 °C; (B) arrows showing sintering of CuNPs from leaf methanol extract. (C,D) show EDX spectra and abundance of Cu.

The EDX measurements unambiguously confirmed the presence of metallic Au in all samples measured. The EDX profile shows a strong Au signal, along with C, O, Al, K, and Ca peaks from the biomolecules on the surface of the AuNPs (Figure 3C,D). These elements may also be present due to the elemental composition of the extracts, from which the AuNPs were not completely purified [34]. The grid on which the samples were examined caused Cu's presence. Thus, all measurement techniques confirmed the presence of AuNPs and NFs. Likewise, the EDX profile of the CuNPs shows strong elemental signals of copper, confirming the presence of CuNPs, as shown in Figure 4C,D. The weight percentages of different elements in the CuNPs were below 10%, as shown in Figure 4C,D. The remaining Wt % was carbon and oxygen present in organic molecules, which act as capping molecules surrounding the nanoparticles, as well as the tape used to mount the CuNPs [35].

2.3. TEM, Particle Size, and Zeta Potential Analysis

The TEM images show NPs from leaf methanol, acetone, and water extracts with protruding petal-like features, which are confirmed to be NFs [36]. As observed in Figures 5A and S4, the particles are spherical dots with an average diameter of 10 nm. An in-depth morphological analysis suggests that the formation of AuNFs occurs by the initial formation of NPs, followed by rapid anisotropic growth, then assembly into a flower shape by secondary reduction at their interface [36]. The rapid color change from yellow to gray without intermediate colors supports this theory of their progression [36]. Thus, we proposed the formation mechanism to be aggregation-based growth, as illustrated in Figure S5. Their three-dimensional orientation gives AuNFs better suspension stability and a greater surface area than spherical AuNPs [37,38]. Also, a significant enhancement of the local electrostatic fields and "petals" are advantageous in catalytic reactions, drug delivery, and nuclear medicine [38]. The size of the NFs from *L. discolor* varies from 30 to 97 nm, with an average size of 67 nm. Borah et al. reported similar sizes using *Syzygium cumini* [39]. Onmaz et al. reported NFs of sizes < 100 nm using *Helichrysum italicum* [40]. Other studies suggest that tannin-based polymers enhance reduction [41], explaining the unexpected formation of NFs from *L. discolor*. NFs can potentially be used to develop biosensors, such that, through surface modification, a color change can confirm their interactions with biomolecules of interest [41]. A familiar example of NFs used in sensing is the home pregnancy test that detects pregnancy (β -HCG hormone) and confirms its presence by a change in color of the test solution [42]. In other studies, the gray suspension of AuNFs was obtained by chemical synthesis, where trisodium citrate and water-soluble polymer were added to HAuCl_4 [43,44]. Moving to a greener synthesis of NFs, using *L. discolor* leaves may be less tedious and more environmentally friendly. Under the given conditions, spherical AuNPs were formed from stem and root methanol, acetone, and water extracts ranging from 10 to 33 and 9.3 to 37.5 nm, respectively (Figure 5B), with smaller sizes (Figure 5D) than the NFs obtained in the leaf samples. Shabestariana et al. acquired spherical AuNPs with an average size of 20.83 nm from *Rhus coriaria* L. (sumac), confirming that significant molecules in the extracts act as ligands that control NP growth [45,46]. Similarly, Donga et al. reported even smaller-sized NPs from *Mangifera indica* ranging from 12.33 to 24.05 nm [47]. Comparably, Pechyen et al. reported similar-sized spherical AuNPs from *Spondias dulcis* [11]. The Figure 5B insets show triangular and hexagonal NPs, which were acquired from acetone stem and root extracts and have been reported by Song et al. to be caused by low concentrations of extracts [48]. However, the effect on the size and shape of AuNPs in the present study may be in response to the plant part and solvent used in extraction, indicating the uniqueness of the phytochemicals in the extracts and their specific requirements for higher temperatures to initiate the reduction process and produce other morphologies [48].

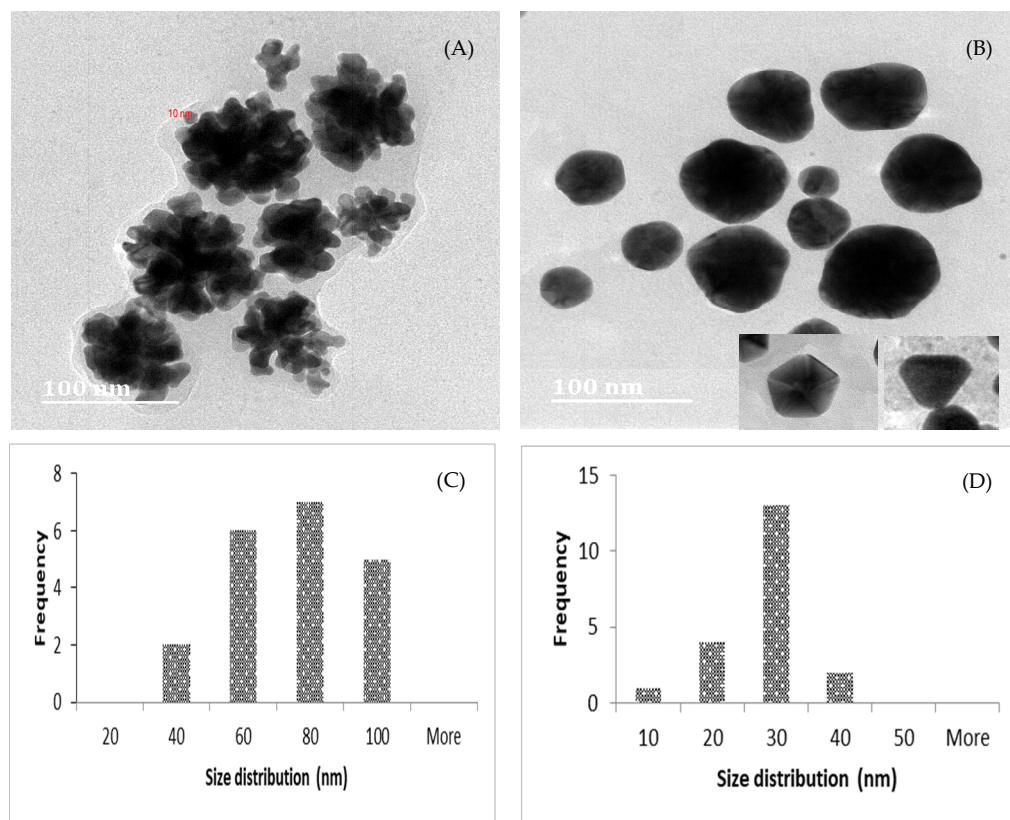


Figure 5. Representative TEM images of the AuNFs (A) from methanol leaf extracts and AuNPs (B) from *L. discolor* methanol stem extract. Insets in B show triangular and hexagonal NPs from stem and root acetone extracts. Histograms show the size distribution of the AuNFs (C) and spherical AuNPs (D).

Figure 6A shows the TEM images of spherical CuNPs from all plant parts and their respective solvents, with particle sizes of 20–104 nm (Figure 6B). In Figure 6A and the inset, NPs are similarly sintered, as observed in Section 2.2. The authors suggest that the large sizes of the CuNPs observed in the present study may be due to the concentration and ability of the biomolecules in the extracts to reduce the volume of the CuSO_4 . Similarly, in a study by Amjad et al., copper nanoparticle size increased with smaller concentrations of the precursor salt [49].

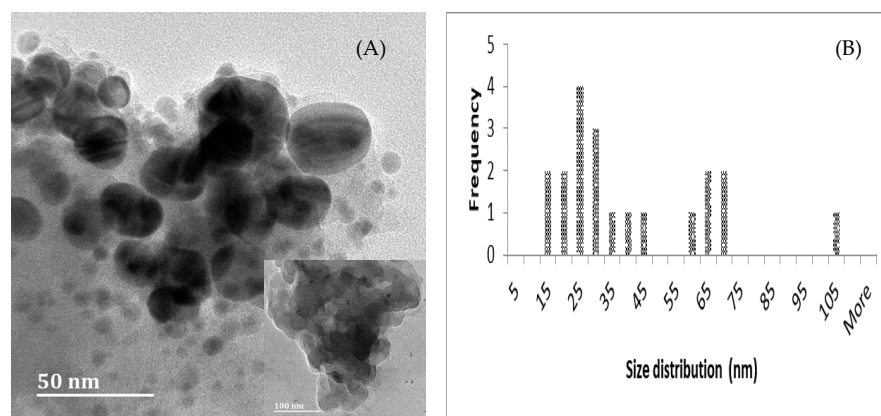


Figure 6. Representative micrograph of (A) CuNPs from stem methanol extract and (B) size distribution. The inset shows a TEM image of sintering in CuNPs exposed to high temperatures.

AuNFs and NPs are soluble in water, suggesting high biofluid solubility and potential as injectables [50]. Their stability may improve the corresponding adsorption of these NPs in the body, which is measured as zeta potential. In addition, the absolute values of zeta potentials for AuNCs were -14.6 , -8.3 , -10.8 , and -6.39 mV, indicating their stability due to the larger electrostatic repulsion [2,51]. CuNPs had a stability range of -43.3 to -13.4 mV. A zeta potential greater than 30 mV or less than -30 mV indicates stable dispersions of NPs in solutions [51].

2.4. FTIR Analysis

FTIR measurements of the NPs were conducted to identify the major functional groups of phytochemicals in *L. discolor* extracts and the AuNFs, NPs, and CuNPs. Strong bands were observed in the methanol, acetone, and water extracts, with peaks corresponding to the O-H stretching of alcohols and carboxylic acids. Similar bands in the extracts were observed to represent alkanes, alkynes, aldehydes, allenes, thiocyanates, and isothiocyanates (Figures S6–S8). The typical FTIR spectra of AuNPs and CuNPs synthesized in the presence of *L. discolor* methanol stem and root extracts, respectively, are shown in Figure 7. Bands at 2780 , 2873 , 2816 , 3015 , 3255 , 3272 , 3299 , and 3313 cm^{-1} are due to N-H stretching of both amines and amides and/or to O-H stretching of alcohols, phenols, or carboxylic acids. The aromatic stretches (C-H) observed at peaks 1894 , 1935 , 1938 , 1954 , 1973 , and 1994 cm^{-1} in the AuNPs and CuNPs may be among the main capping agents. The binding characteristics of amino groups in the samples could cause the CuNPs to aggregate, which resulted in sintering [52,53].

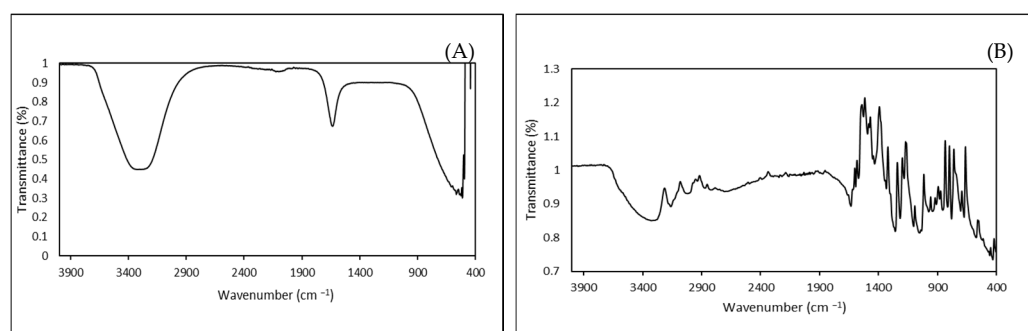


Figure 7. FTIR spectrum of AuNPs from methanol stem extract (A) and CuNPs from methanol root extract (B) from *Lannea discolor*.

2.5. The Antibacterial Activity of AuNPs and CuNPs

In addition to the previously mentioned applications, NPs may be a potent antibacterial agent. Although extensive research from the literature has been devoted to proving the antibacterial activity of other metal-based NPs [54], the focus on the antibacterial activity of AuNPs/NFs and CuNPs is limited; as such, the present study contributes hugely. MIC was employed to estimate the inhibition AuNPs/NFs and CuNPs may have on microorganisms. The MICs for the AuNPs and NFs are summarized in Table 1. Interestingly, the MIC values of the NPs were similar for the bacterial strains. *Staphylococcus aureus* (ATCC 25923), *Pseudomonas aeruginosa* (ATCC 27853), and *Bacillus subtilis* (ATCC 6633) were the most susceptible to AuNFs from all extracts (leaf, stem, and root) and solvents (methanol, acetone, and water) at both 25 °C and 80 °C and showed the lowest viability compared to *Klebsiella pneumoniae* (ATCC 700603) and *Escherichia coli* (ATCC 25922). The authors attributed the activity of the AuNFs to the high aspect ratio of the elongated petal-like surfaces, which induce localized tension and increase reactive oxygen species, thus causing bacterial membrane rupture [55]. Additionally, the enhancement of *L. discolor* extracts by NPs improves the ability to disrupt the bacterial cell membrane [55]. The MICs from the NPs from stem and root methanol, acetone, and water extracts were similar and exhibited good antibacterial activity against all the bacteria due to their similar sizes. Contrastingly,

all the crude extracts displayed antibacterial activity at only 1000 µg/mL, explaining the significance of nanoparticle enhancement.

Table 1. Antibacterial activity of AuNPs and NFs containing *Lannea discolor* extracts.

| | AuNFs and NPs (µg/mL) | | | | | | | | | | | | | | | | Extracts (µg/mL) | G | HAuCl ₄ (1 mM) | | |
|----------------------|-----------------------|-------|-------|-------|-------|-------|-------|-------|-------|-------|-------|------|------|------|-------|-------|------------------|------|---------------------------|-----|------|
| | 37 | 38 | 39 | 40 | 41 | 42 | 43 | 44 | 45 | 46 | 47 | 48 | 49 | 50 | 51 | 52 | | | | 53 | 54 |
| <i>P. aeruginosa</i> | 250 | 125 | 62.5 | 62.5 | 62.5 | 62.5 | 62.5 | 62.5 | 62.5 | 125 | 62.5 | 7.81 | 500 | 500 | 500 | 500 | 1000 | 1000 | 1000 | 7.8 | 500 |
| <i>K. pneumoniae</i> | 250 | 125 | 125 | 250 | 250 | 250 | 250 | 62.5 | 125 | 15.62 | 15.62 | 1000 | 1000 | 0 | 0 | 7.81 | 62.5 | 0 | 1000 | 7.8 | 500 |
| <i>E. coli</i> | 250 | 125 | 1000 | 500 | 125 | 62.5 | 15.62 | 15.62 | 125 | 125 | 125 | 500 | 500 | 500 | 500 | 31.25 | 31.25 | 0 | 1000 | 7.8 | 500 |
| <i>B. subtilis</i> | 250 | 31.25 | 31.25 | 31.25 | 31.25 | 31.25 | 31.25 | 31.25 | 15.62 | 62.5 | 62.5 | 62.5 | 62.5 | 62.5 | 15.62 | 15.62 | 7.81 | 0 | 1000 | 7.8 | 1000 |
| <i>S. aureus</i> | 62.5 | 62.5 | 0 | 62.5 | 62.5 | 0 | 15.62 | 62.5 | 125 | 250 | 250 | 500 | 500 | 250 | 500 | 250 | 250 | 0 | 1000 | 7.8 | 1000 |

Sample keys: 37 = Au_ML_25 °C; 38 = Au_MS_25 °C; 39 = Au_MR_25 °C; 40 = Au_ML_80 °C; 41 = Au_MS_80 °C; 42 = Au_MR_80 °C; 43 = Au_AL_25 °C; 44 = Au_AS_25 °C; 45 = Au_AR_25 °C; 46 = Au_AL_80 °C; 47 = Au_AS_80 °C; 48 = Au_AR_80 °C; 49 = Au_WL_25 °C; 50 = Au_WS_25 °C; 51 = Au_WR_25 °C; 52 = Au_WL_80 °C; 53 = Au_WS_80 °C; 54 = Au_WR_80 °C; G = gentamicin; HAuCl₄ = gold(III) chloride hydrate.

Reports show that the antibacterial activity of AuNPs is associated with their surface modifications, such as the shape and the molecules involved in capping the NPs during synthesis [55]. Some bacterial strains, like *S. aureus*, are considered threatenful to humans; hence, introducing AuNPs as antibacterial agents is fundamental. Morphological interactions depend on surface orientations to enhance antibacterial activity [56]. NPs with edges rupture the membrane of bacteria and disrupt them. Many experiments on nanoscale surfaces have observed the morphological interactions of AuNPs/NFs with bacteria, confirming the significance of surface orientation for activity [56,57]. In the present study, the high activity can be attributed to the large surface area and disruptive ability of AuNPs/NFs. Studies have also ascribed the high activity of gold NPs against Gram (−) bacteria to the thin peptidoglycan membrane, and that lower activity is usually observed in Gram (+) bacteria with a peptidoglycan membrane with a thickness that is 50% higher [58]. However, this is not the case in this study, as activity varies equitably within the Gram (−) and Gram (+) bacteria. Similarly, several other studies have observed impressive antibacterial activity from AuNPs in both Gram (−) and Gram (+) bacteria [59–61]. The total MIC for different extracts resembling that of AuCl₄ confirms that the activity of phytochemicals improves when incorporated into different nanoformulations. The outcome demonstrates that the AuNPs/NFs synthesized from *L. discolor* can inhibit the growth of the tested bacteria even at low concentrations. The CuNPs in this work showed no activity against the tested bacteria, ideally indicated by a change in color after adding Resazurin. This is attributed to the sintered NPs that could not interact with the bacterial cells as they are more of a solid mass instead of polydispersed. Other causes may include the size, shape, specific surface area, and surface curvature of the nanoparticles [62]. However, CuNPs in other studies have shown comparable activity in contrast to their counterparts [63]. A higher concentration of precursor salts and a longer incubation period may produce CuNPs with better antibacterial activity. All these data reported here support using the *L. discolor* extracts as an alternative to toxic chemical reductants in producing AuNPs, NFs, and CuNPs that can inhibit the growth of different bacteria.

3. Materials and Methods

3.1. Collection of Plant Material

Lannea discolor material was collected from Vuwani (Vhembe district) (23°09′42.9″ S 30°25′22.6″ E) in November 2018. The plant species were identified by U.R. with the aid of the literature, and online herbariums (<https://plants.jstor.org/compilation>; <https://powo.science.kew.org>) (Accessed on 5 November 2018) and voucher specimens (UR 01) were prepared and deposited at the University of Venda Herbarium (UVH) in

South Africa. *Lanenea discolor* material reserved for experiments was air-dried, ground with a pestle and mortar, and stored for further use.

Extraction

The air-dried material was ground into a fine powder using a grinding mill (NETZSCH, Selb, Germany). The extracts were obtained by maceration for three 3-day periods at a ratio of 1:10 for solvents, methanol, acetone, and water. They were filtered using filter paper (Whatman No. 1), evaporated to dryness, and stored at 4 °C for subsequent tests.

3.2. Synthesis of Nanoparticles

AuNPs and CuNPs were synthesized using *Lanenea discolor* (10 mg/mL) extracts. After dissolving 250 mg of gold precursor in 50 mL of distilled water, a stock solution of gold (III) chloride hydrate ($\text{HAuCl}_4 \cdot \text{aq}$) with a concentration of 14 mM. (Millipore, Merck) was prepared. After, the stock solution was diluted to a concentration of 1 mM HAuCl_4 . The addition of 10 mL of *Lanenea discolor* extract to a mixture containing 40 mL of 1 mM HAuCl_4 solution was incubated at 25 °C and 80 °C for an hour, then in the dark for twenty-four hours. The hue of the solution changed, indicating AuNP formation. The mixture was centrifuged for ten minutes at 10,000 rpm after being washed twice with distilled water. AuNP pellets were gathered, air-dried, and kept at 4 °C.

To synthesize CuNPs, 1 mM copper (II) sulfate (CuSO_4) was made in distilled water, after which 10 mL of *L. discolor* extracts was added to 40 mL of copper sulfate solution (1 mM) and incubated at 25 °C and 80 °C for one hour. The color of the mixtures changed, indicating the formation of CuNPs. After twenty-four hours, the nanoparticles were rinsed twice with distillation water and centrifuged at 12,000 rpm for 15 min. CuNP pellets were dried at 60 °C overnight and then stored at 4 °C for future use.

3.3. Characterization

3.3.1. Physicochemical Characterization of AuNPs and CuNPs

UV-Vis spectroscopy analysis recorded the absorbance of AuNPs and CuNPs in 96-well plates containing 160 μL of NPs using a SpectraMax M3 spectrophotometer (Molecular Devices, Sunnyvale, CA, USA) at wavelengths of 200–800 nm and a scan speed of 200 nm/min.

3.3.2. Scanning Electron Microscopy Analysis and Energy-Dispersive X-ray Microanalysis

The AuNPs and CuNPs were sonicated for 20 min, after which about 40 μL of each sample was mounted on a glass coverslip attached to a brass stub with adhesive carbon tape and dried under a mercury lamp for about 60 min. The NPs were made conductive with a layer of gold (ca. 25 nm) using an automated Quorum (Q15OR ES) Module sputter coater (vacuum of 0.1 Torr for 2.5 min) and examined at varying magnifications, using a Zeiss Ultra-Plus FEG-SEM at an acceleration voltage of 5 kV. The images were captured with NIS-D image software (AzTec analysis software, V. 1.2, Oxford Instruments, High Wycombe, UK). At the same time, elemental analysis was performed with an energy-dispersive X-ray spectrometer (EDX), coupled to an Astronomical Thermal Emission Camera (Aztec) version 1.2 at 20 kV.

3.3.3. Transmission Electron Microscopy Analysis and Measurements of Zeta Potential

Carbon-coated 200-mesh copper grids were used to scoop a portion of the AuNPs and CuNPs and dried under a mercury lamp for about 30 min before analysis. The morphology and size of the nanoparticles were determined using a JEOL JEM-2100 TEM at an acceleration voltage of 200 kV.

Zeta analysis was used to measure the surface charge of the NPs using a Zetasizer Nano-Zs90 (Malvern International Ltd., MPT-Z, Malvern, London, UK). For each sample, the mean diameter \pm SD for ten runs was calculated by applying a multimodal animation.

3.3.4. Fourier-Transform Infrared Spectroscopy (FTIR) Analysis

The ATR-IR FTIR (Alpha 1; Bruker, Germany, Europe) was used to describe the chemically possible compound interactions. The samples were developed and evaluated at a 4000–400 cm^{-1} scan range. The spectra were interpreted by comparing the spectral data with references from identifying functional groups in the literature [64].

3.4. Antibacterial Assay

The antibacterial activity of the NPs, gentamicin, crude extracts, HAuCl_4 and CuSO_4 solutions was studied against *Staphylococcus aureus* (ATCC 25923) and *Escherichia coli* (ATCC 25922), *Pseudomonas aeruginosa* (ATCC 27853), *Klebsiella pneumoniae* (ATCC 700603) and *Bacillus subtilis* (ATCC 6633) using a minimum inhibitory concentration assay (MIC). A 96-well microtiter plate (Tarsons, Kolkata, India) was prepared by transferring 160 μL of Mueller–Hinton broth to the first row and 100 μL to the second row, under a laminar airflow chamber. A volume of 40 μL of NPs, extract, and gentamicin was added to the first row of the plate, followed by 10 μL of bacterial inoculum. After this, serial dilutions with concentration 7.8–1000 $\mu\text{g}/\text{mL}$ were performed, 100 μL of bacteria was added, and the plates were placed for twenty-four hours at 37 °C for incubation. Upon removal, 10 μL of Resazurin solution, as per Madikizela et al., was added to each well, followed by a further 30 min incubation to determine the MIC value by the observed color change [65].

4. Conclusions

In the current study, the straightforward synthesis of AuNPs, NFs, and CuNPs was reported for the first time, employing *L. discolor* leaves, stem, and root extracts in a more cost-effective, green technique. The ability of the functional groups in the phytochemicals of the organs of *L. discolor* to function as a reducing and capping agent is linked to the formation of AuNFs and NPs as well as spherical CuNPs. TEM micrographs provided evidence toward the morphology of AuNPs with several shapes, including flowers, from methanol, acetone, and water leaf extracts, while spherical, triangular, and hexagonal AuNPs were observed in the stems and root of all solvents from which extracts were acquired. Due to their merged surface area, the sintered CuNPs from the leaf, stem, and root extracts can potentially find a unique position in many technological applications, such as sensors, flexible devices, and conductivity. Despite the noticeable bacterial activity of AuNPs and NFs, more study is required into their intricate cytotoxicity profiles. Critical parameters for synthesizing the AuNFs and NPs in this study include the concentration and ratio of gold/leaf, stem and root extracts, time, and temperature. The techniques used in this study present several significant advantages, such as biocompatibility, multifunctionality, and economic viability. On the other hand, there may be a need to optimize techniques to produce AuNFs and sintered CuNPs from *L. discolor*, which could be exploited to develop novel extract-formulated nanoparticles with prospective applications in different fields.

Supplementary Materials: The following supporting information can be downloaded at: <https://www.mdpi.com/article/10.3390/inorganics12020036/s1>, Figure S1: The UV-Vis data of AuNFs, NPs (A,B) and CuNPs (C,D). Legends denote extracts from which nanoparticles were synthesized; Figure S2: SEM micrographs of AuNFs and AuNPs synthesized from leaf, stem and root methanol (A–C), acetone (D–F) and water (G–I) extracts, of *Lannea discolor*; Figure S3: Representative SEM images of CuNPs from *Lannea discolor* leaf, stem and root methanol (A–C), acetone (D–F) and water (G–H) extracts; Figure S4: TEM images of the synthesized AuNFs and AuNPs. (A,D,G) show AuNFs synthesized from leaf methanol, acetone, and water extracts, respectfully. AuNPs synthesized from methanol, acetone, and water stem and roots extracts are shown in micrographs (B,C,E,F,H,I); Figure S5: Schematic diagram showing proposed growth mechanism of AuNFs from *Lannea discolor* leaves; Figure S6: FTIR spectra of *Lannea discolor* leaf (A), stem (B) and root (C) crude methanol extracts; Figure S7: FTIR spectra of *Lannea discolor* leaf (A), stem (B) and root (C) crude acetone extracts; Figure S8 FTIR spectra of *Lannea discolor* leaf (A), stem (B) and root (C) crude water extracts.

Author Contributions: Conceptualization, U.R. and N.A.M.; methodology, U.R.; formal analysis, U.R.; investigation, U.R.; data curation, U.R.; writing—original draft preparation, U.R. and N.A.M.; writing—review and editing, U.R. and N.A.M.; validation, N.A.M.; visualization, U.R.; project administration, N.A.M.; supervision, N.A.M. and A.S.; resources, N.A.M. and A.S. All authors have read and agreed to the published version of the manuscript.

Funding: This work was supported by the National Research Foundation (Grant: UID 112386).

Data Availability Statement: The data presented in this study are available in this article and Supplementary Material.

Acknowledgments: The authors thank the Faculty of Science Engineering and Agriculture, University of Venda, South Africa, for providing the resources needed to conduct the research and the University of KwaZulu-Natal Westville Campus Microscopy and Microanalysis unit for facilities. The authors would like to express their sincere gratitude to N.A Akwu (Preclinical Drug Development Platform, Faculty of Health Sciences, North-West University) for her invaluable contribution to the preparation of this manuscript.

Conflicts of Interest: The authors declare no conflicts of interest.

References

1. Malike, S.; Muhammad, K.; Waheed, Y. Nanotechnology: A revolution in modern industry. *Molecules* **2023**, *28*, 661. [[CrossRef](#)]
2. Khan, I.; Saeed, K.; Khan, I. Nanoparticles: Properties, applications, and toxicities. *Arab. J. Chem.* **2019**, *12*, 908–931. [[CrossRef](#)]
3. Szczyglewska, P.; Feliczak-Guzik, A.; Nowak, I. Nanotechnology—General Aspects: A Chemical Reduction Approach to the Synthesis of Nanoparticles. *Molecules* **2023**, *28*, 4932. [[CrossRef](#)] [[PubMed](#)]
4. Singh, J.; Dutta, T.; Kim, K.H.; Rawat, M.; Samddar, P.; Kumar, P. Green synthesis of metals and their oxide nanoparticles: Applications for environmental remediation. *J. Nanobiotechnol.* **2018**, *16*, 84. [[CrossRef](#)] [[PubMed](#)]
5. Egorova, K.S.; Ananikov, V.P. Which metals are green for catalysis? Comparison of the toxicities of Ni, Cu, Fe, Pd, Pt, Rh, and Au salts. *Angew. Chem. Int. Ed.* **2016**, *55*, 12150–12162. [[CrossRef](#)]
6. Louis, C.; Pluchery, O. *Gold Nanoparticles in the Past: Before the Nanotechnology Era Gold Nanoparticles for Physics, Chemistry, and Biology*; World Scientific Publishing: Singapore, 2012; pp. 1–28.
7. Chiang, M.C.; Nicol, C.J.; Lin, C.H.; Chen, S.J.; Yen, C.; Huang, R.N. Nanogold induces anti-inflammation against oxidative stress induced in human neural stem cells exposed to amyloid-beta peptide. *Neurochem. Int.* **2021**, *145*, 104992. [[CrossRef](#)] [[PubMed](#)]
8. Leary, J. *Attaching Biomolecules to Nanoparticles*; Cambridge University Press: Cambridge, UK, 2022; pp. 103–121.
9. Kulkarni, D.; Sherkar, R.; Shirsathe, C.; Sonwane, R.; Varpe, N.; Shelke, S.; More, M.P.; Pardeshi, S.R.; Dhaneshwar, G.; Junnuthula, V.; et al. Biofabrication of nanoparticles: Sources, synthesis, and biomedical applications. *Front. Bioeng. Biotechnol.* **2023**, *11*, 1159193. [[CrossRef](#)] [[PubMed](#)]
10. Shen, D.S.; Joseph, M.; Daizy, P. Phytosynthesis of Au, Ag and Au-Ag bimetallic nanoparticles using aqueous extract and dried leaf of *Anacardium occidentale*. *Spectrochim. Acta Part A Mol. Biomol. Spectrosc.* **2011**, *79*, 254. [[CrossRef](#)]
11. Pechyen, C.; Ponsanti, K.; Tangnorawich, B.; Ngernyuang, N. Biogenic synthesis of gold nanoparticles mediated by *Spondias dulcis* (Anacardiaceae) peel extract and its cytotoxic activity in human breast cancer cell. *Toxicol. Rep.* **2022**, *9*, 1092. [[CrossRef](#)]
12. Alhumaydhi, F.A. Green synthesis of gold nanoparticles using extract of *Pistacia chinensis* and their in vitro and in vivo biological activities. *J. Nanomater.* **2022**, *1*, 11. [[CrossRef](#)]
13. Crisan, M.C.; Teodora, M.; Lucian, M. Copper nanoparticles: Synthesis and characterization, physiology, toxicity, and antimicrobial applications. *Appl. Sci.* **2021**, *12*, 141. [[CrossRef](#)]
14. Athanassiou, E.K.; Grass, R.N.; Stark, W.J. Large-scale production of carbon-coated copper nanoparticles for sensor applications. *Nanotechnology* **2006**, *17*, 1668. [[CrossRef](#)] [[PubMed](#)]
15. Zhou, Q.; Zhou, M.; Li, Q.; Wang, R.; Fu, Y.; Jiao, T. Facile biosynthesis and grown mechanism of gold nanoparticles in *Pueraria lobata* extract. *Colloids Surf. A Physicochem. Eng.* **2019**, *567*, 69. [[CrossRef](#)]
16. Martínez-Vieyra, C.; Olguin, M.T.; Gutiérrez-Segura, E.; López-Tellez, G. Comparison of Ag, Cu and Zn nanoparticles obtained using *Aloe vera* extract and gamma ionizing radiation. *J. Appl. Res. Technol.* **2020**, *18*, 289–314.
17. Wu, S.; Rajeshkumar, S.; Madasamy, M.; Mahendran, V. Green synthesis of copper nanoparticles using *Cissus vitifolia* and its antioxidant and antibacterial activity against urinary tract infection pathogens. *Artif. Cells Nanomed. Biotechnol.* **2020**, *48*, 1153. [[CrossRef](#)] [[PubMed](#)]
18. Varghese, B.; Kurian, M.; Krishna, S.; Athira, T.S. Biochemical synthesis of copper nanoparticles using *Zingiber officinalis* and *Curcuma longa*: Characterization and antibacterial activity study. *Mater. Today Proc.* **2020**, *25*, 302. [[CrossRef](#)]
19. Sundaram, C.S.; Kumar, J.S.; Kumar, S.S.; Ramesh, P.L.N.; Zin, T.; Rao, U.M. 2020 Antibacterial and anticancer potential of *Brassica oleracea var acephala* using biosynthesised copper nanoparticles. *Med. J. Malays.* **2020**, *75*, 677.
20. Shubhashree, K.R.; Reddy, R.; Gangula, A.K.; Nagananda, G.S.; Badiya, P.K.; Ramamurthy, S.S.; Reddy, N. Green synthesis of copper nanoparticles using aqueous extracts from *Hyptis suaveolens* (L). *Mater. Chem. Phys.* **2022**, *280*, 125795. [[CrossRef](#)]

21. Maroyi, A. *Lannea discolor* its botany, ethnomedicinal uses, phytochemistry, and pharmacological properties. *Asian. J. Pharm. Clin. Res.* **2018**, *11*, 49. [[CrossRef](#)]
22. Mwamatope, B.; Tembo, D.; Kampira, E.; Maliwichi-Nyirenda, C.; Ndolo, V. Seasonal variation of phytochemicals in four selected medicinal plants. *Pharmacogn. Res.* **2021**, *13*, 218. [[CrossRef](#)]
23. Abdallah, B.M.; Ali, E.M. Therapeutic Potential of Green Synthesized Gold Nanoparticles Using Extract of *Leptadenia hastata* against Invasive Pulmonary Aspergillosis. *J. Fungi* **2022**, *8*, 442. [[CrossRef](#)] [[PubMed](#)]
24. Liu, K.; He, Z.; Curtin, J.F.; Byrne, H.J.; Tian, F. A novel, rapid, seedless, in situ synthesis method of shape and size controllable gold nanoparticles using phosphates. *Sci. Rep.* **2019**, *9*, 7421. [[CrossRef](#)]
25. Liebig, F.; Henning, R.; Sarhan, R.M.; Prietzel, C.; Bargheer, M.; Koetz, J. A new route to gold nanoflowers. *Nanotechnology* **2018**, *29*, 185603. [[CrossRef](#)] [[PubMed](#)]
26. Gao, L.; Mei, S.; Ma, H.; Chen, X. Ultrasound-assisted green synthesis of gold nanoparticles using citrus peel extract and their enhanced anti-inflammatory activity. *Ultrason. Sonochem.* **2022**, *83*, 105940. [[CrossRef](#)] [[PubMed](#)]
27. Mthembu, S.B.; Akintayo, D.C.; Moodley, B.; Gumbi, B.P. Development of gold plasmonic nanoparticles for detection of polydiallyldimethylammonium chloride at Umgeni water treatment plants: An optimised study and case application. *Heliyon* **2023**, *9*, e17136. [[CrossRef](#)] [[PubMed](#)]
28. Das, P.E.; Abu-Yousef, I.A.; Majdalawieh, A.F.; Narasimhan, S.; Poltronieri, P. Green synthesis of encapsulated copper nanoparticles using a hydroalcoholic extract of *Moringa oleifera* leaves and assessment of their antioxidant and antimicrobial activities. *Molecules* **2022**, *25*, 555. [[CrossRef](#)] [[PubMed](#)]
29. Kim, H.S.; Lee, D.Y. Near-infrared-responsive cancer photothermal and photodynamic therapy using gold nanoparticles. *Polymers* **2018**, *10*, 961. [[CrossRef](#)]
30. Peng, C.; Tong, H.; Yuan, P.; Sun, L.; Jiang, L.; Shi, J. Aggregation, Sedimentation, and Dissolution of Copper Oxide Nanoparticles: Influence of Low-Molecular-Weight Organic Acids from Root Exudates. *Nanomaterials* **2019**, *9*, 841. [[CrossRef](#)]
31. Babalola, B.J.; Ayodele, O.O.; Olubambi, P.A. Sintering of nanocrystalline materials: Sintering parameters. *Heliyon* **2023**, *9*, e14070. [[CrossRef](#)]
32. Hong, G.B.; Wang, J.F.; Chuang, K.J.; Cheng, H.Y.; Chang, K.C.; Ma, C.M. Preparing copper nanoparticles and flexible copper conductive sheets. *Nanomaterials* **2022**, *12*, 360. [[CrossRef](#)]
33. Sarwax, N.; Choi, S.H.; Dastgeer, G.; Humayoun, U.B.; Kumar, M.; Nawaz, A.; Jeong, D.I.; Zaidi, S.F.; Yoon, D.H. Synthesis of citrate-capped copper nanoparticles: A low temperature sintering approach for the fabrication of oxidation stable flexible conductive film. *Appl. Surf. Sci.* **2021**, *542*, 148609. [[CrossRef](#)]
34. Keskin, C.; Atalar, M.N.; Firat Baran, M.; Baran, A. Environmentally friendly rapid synthesis of gold nanoparticles from *Artemisia absinthium* plant extract and application of antimicrobial activities. *J. Inst. Sci. Technol.* **2021**, *11*, 365. [[CrossRef](#)]
35. Ismail, M.; Gul, S.; Khan, M.I.; Khan, M.A.; Asiri, A.M.; Khan, S.B. Green synthesis of zerovalent copper nanoparticles for efficient reduction of toxic azo dyes congo red and methyl orange. *Green Process. Synth.* **2019**, *8*, 135. [[CrossRef](#)]
36. Sajanlal, P.R.; Sreeprasad, T.S.; Samal, A.K.; Pradeep, T. Anisotropic nanomaterials: Structure, growth, assembly, and functions. *Nano Rev.* **2011**, *2*, 5883. [[CrossRef](#)]
37. Jakhmola, A.; Vecchione, R.; Gentile, F.; Profeta, M.; Manikas, A.C.; Battista, E.; Netti, P.A. Experimental and theoretical study of biodirected green synthesis of gold nanoflowers. *Mater. Today Chem.* **2019**, *14*, 100203. [[CrossRef](#)]
38. Ji, Y.; Ren, M.; Li, Y.; Huang, Z.; Shu, M.; Yang, H.; Xiong, Y.; Xu, Y. Detection of aflatoxin B1 with immunochromatographic test strips: Enhanced signal sensitivity using gold nanoflowers. *Talanta* **2015**, *142*, 206. [[CrossRef](#)]
39. Borah, D.; Hazarika, M.; Tailor, P.; Silva, A.R.; Chetia, B.; Singaravelu, G.; Das, P. Starch-templated biosynthesis of gold nanoflowers for in vitro antimicrobial and anticancer activities. *Appl. Nanosci.* **2018**, *8*, 241. [[CrossRef](#)]
40. Onmaz, N.E.; Demirezen Yilmaz, D.; Imre, K.; Morar, A.; Gungor, C.; Yilmaz, S.; Gundog, D.A.; Dishan, A.; Herman, V.; Gungor, G. Green synthesis of gold nanoflowers using *Rosmarinus officinalis* and *Helichrysum italicum* extracts: Comparative studies of their antimicrobial and antibiofilm activities. *Antibiotics* **2022**, *11*, 1466.
41. Deshmukh, A.R.; Kim, B.S. Flower-like biogenic gold nanostructures for improved catalytic reduction of 4-nitrophenol. *J. Environ. Chem. Eng.* **2021**, *9*, 106707. [[CrossRef](#)]
42. Pluchery, O.; Remita, H.; Schaming, D. Demonstrative experiments about gold nanoparticles and nanofilms: An introduction to nanoscience. *Gold Bull.* **2013**, *46*, 319. [[CrossRef](#)]
43. Tanaka, R.; Yuhi, T.; Nagatani, N.; Endo, T.; Kerman, K.; Takamura, Y.; Tamiya, E. A novel enhancement assay for immunochromatographic test strips using gold nanoparticles. *Anal. Bioanal. Chem.* **2006**, *385*, 1414. [[CrossRef](#)]
44. Merza, K.S.; Al-Attabi, H.D.; Abbas, Z.M.; Yusr, H. A Comparative Study on Methods for Preparation of Gold Nanoparticles. *Green. Sustain. Chem.* **2011**, *2*, 26. [[CrossRef](#)]
45. Kariuki, V.M.; Hoffmeier, J.C.; Yazgan, I.; Sadik, O.A. Seedless synthesis and SERS characterization of multi-branched gold nanoflowers using water-soluble polymers. *Nanoscale* **2017**, *9*, 8330. [[CrossRef](#)]
46. Shabestarian, H.; Homayouni-Tabrizi, M.; Soltani, M.; Namvar, F.; Azizi, S.; Mohamad, R.; Shabestarian, H. Green synthesis of gold nanoparticles using *sumac* aqueous extract and their antioxidant activity. *Mater. Res.* **2016**, *20*, 264. [[CrossRef](#)]
47. Donga, S.; Bhadu, G.R.; Chanda, S. Antimicrobial, antioxidant, and anticancer activities of gold nanoparticles green synthesized using *Mangifera indica* seed aqueous extract. *Artif. Cells Nanomed. Biotechnol.* **2020**, *48*, 1315. [[CrossRef](#)]

48. Song, J.Y.; Jang, H.K.; Kim, B.S. Biological synthesis of gold nanoparticles using *Magnolia kobus* and *Diopyros kaki* leaf extracts. *Process Biochem.* **2009**, *44*, 1133. [[CrossRef](#)]
49. Amjad, R.; Mubeen, B.; Ali, S.S.; Imam, S.S.; Alshehri, S.; Ghoneim, M.M.; Alzarea, S.I.; Rasool, R.; Ullah, I.; Nadeem, M.S.; et al. Green Synthesis and Characterization of Copper Nanoparticles Using *Fortunella margarita* Leaves. *Polymers* **2021**, *13*, 4364. [[CrossRef](#)]
50. Chopra, H.; Bibi, S.; Singh, I.; Hasan, M.M.; Khan, M.S.; Yousaf, Q.; Baig, A.A.; Rahman, M.M.; Islam, F.; Emran, T.B.; et al. Green metallic nanoparticles: Biosynthesis to applications. *Front. Bioeng. Biotechnol.* **2022**, *10*, 548. [[CrossRef](#)]
51. Patra, J.K.; Das, G.; Fraceto, L.F.; Campos, E.V.; Rodriguez-Torres, M.D.; Acosta-Torres, L.S.; Diaz-Torres, L.A.; Grillo, R.; Swamy, M.K.; Sharma, S.; et al. Nano based drug delivery systems: Recent developments and future prospects. *J. Nanobiotechnol.* **2018**, *16*, 71. [[CrossRef](#)]
52. Gawande, M.B.; Goswami, A.; Felpin, F.X.; Asefa, T.; Huang, X.; Silva, R.; Zou, X.; Zboril, R.; Varma, R.S. Cu and Cu-based nanoparticles: Synthesis and applications in catalysis. *Chem. Rev.* **2016**, *116*, 3722–3811. [[CrossRef](#)]
53. Sizochenko, N.; Mikolajczyk, A.; Syzochenko, M.; Puzyn, T.; Leszczynski, J. Zeta potentials (ζ) of metal oxide nanoparticles: A meta-analysis of experimental data and a predictive neural network modeling. *NanolImpact* **2021**, *22*, 100317. [[CrossRef](#)]
54. Murthy, H.C.; Desalegn, T.; Kassa, M.; Abebe, B.; Assefa, T. Synthesis of green copper nanoparticles using medicinal plant *Hagenia abyssinica* (Brace) JF Gmel leaf extract: Antimicrobial properties. *J. Nanomater.* **2020**, *1*, 3924081. [[CrossRef](#)]
55. Yu, Z.; Li, Q.; Wang, J.; Yu, Y.; Wang, Y.; Zhou, Q.; Li, P. Reactive oxygen species-related nanoparticle toxicity in the biomedical field. *Nanoscale Res. Lett.* **2020**, *15*, 115. [[CrossRef](#)]
56. Yougbare, S.; Chang, T.K.; Tan, S.H.; Kuo, J.C.; Hsu, P.H.; Su, C.Y.; Kuo, T.R. Antimicrobial gold nanoclusters: Recent developments and future perspectives. *Int. J. Mol. Sci.* **2019**, *20*, 2924. [[CrossRef](#)]
57. Mousavi, S.M.; Zarei, M.; Hashemi, S.A.; Ramakrishna, S.; Chiang, W.H.; Lai, C.W.; Gholami, A. Gold nanostars-diagnosis, bioimaging and biomedical applications. *Drug Metab. Rev.* **2020**, *52*, 299. [[CrossRef](#)]
58. Okkeh, M.; Bloise, N.; Restivo, E.; De Vita, L.; Pallavicini, P.; Visai, L. Gold nanoparticles: Can they be the next magic bullet for multidrug-resistant bacteria? *Nanomaterials* **2021**, *11*, 312. [[CrossRef](#)]
59. Umadevi, M.; Rani, T.; Balakrishnan, T.; Ramanibai, R. Antimicrobial activity of silver nanoparticles under an ultrasonic field. *Int. J. Pharm. Sci. Nanotechnol.* **2011**, *4*, 1491.
60. Zheng, K.; Setyawati, M.I.; Leong, D.T.; Xie, J. Antimicrobial Gold Nanoclusters. *ACS Nano* **2017**, *11*, 6904. [[CrossRef](#)]
61. Rovati, D.; Albini, B.; Galinetto, P.; Grisoli, P.; Bassi, B.; Pallavicini, P.; Dacarro, G.; Taglietti, A. High Stability Thiol-Coated Gold Nanostars Monolayers with Photo-Thermal Antibacterial Activity and Wettability Control. *Nanomaterials* **2019**, *9*, 1288. [[CrossRef](#)]
62. Montes de Oca-Vásquez, G.; Solano-Campos, F.; Vega-Baudrit, J.R.; López-Mondéjar, R.; Odriozola, I.; Vera, A.; Moreno, J.L.; Bastida, F. Environmentally relevant concentrations of silver nanoparticles diminish soil microbial biomass but do not alter enzyme activities or microbial diversity. *J. Hazard. Mater.* **2020**, *391*, 122224. [[CrossRef](#)]
63. Qamar, H.; Rehman, S.; Chauhan, D.K.; Tiwari, A.K.; Upmanyu, V. Green Synthesis, Characterization and Antimicrobial Activity of Copper Oxide Nanomaterial Derived from *Momordica charantia*. *Int. J. Nanomed.* **2020**, *15*, 2541–2553. [[CrossRef](#)] [[PubMed](#)]
64. Coates, J. Interpretation of infrared spectra, a practical approach. In *Encyclopedia of Analytical Chemistry*; Meyers, R.A., Ed.; John Wiley & Sons, Ltd.: Hoboken, NJ, USA, 2000; p. 10815.
65. Madikizela, B.; Ndhlala, A.R.; Finnie, J.F.; Staden, J.V. In vitro antimicrobial activity of extracts from plants used traditionally in South Africa to treat tuberculosis and related symptoms. *Evid. Based Complement. Altern. Med.* **2013**, *1*, 840719.

Disclaimer/Publisher's Note: The statements, opinions and data contained in all publications are solely those of the individual author(s) and contributor(s) and not of MDPI and/or the editor(s). MDPI and/or the editor(s) disclaim responsibility for any injury to people or property resulting from any ideas, methods, instructions or products referred to in the content.